

Omnidirectional excitation of sidewall gap-plasmons in a hybrid gold-nanoparticle/aluminum-nanopore structure

Chatdanai Lumdee¹ and Pieter G. Kik^{1,2,a}

¹CREOL, The College of Optics and Photonics, University of Central Florida, 4000 Central Florida Blvd., Orlando, Florida 32816, USA

²Physics Department, University of Central Florida, 4000 Central Florida Blvd., Orlando, Florida 32816, USA

(Received 19 January 2016; accepted 13 March 2016; published online 6 June 2016)

The gap-plasmon resonance of a gold nanoparticle inside a nanopore in an aluminum film is investigated in polarization dependent single particle microscopy and spectroscopy. Scattering and transmission measurements reveal that gap-plasmons of this structure can be excited and observed under normal incidence excitation and collection, in contrast to the more common particle-on-a-mirror structure. Correlation of numerical simulations with optical spectroscopy suggests that a local electric field enhancement factor in excess of 50 is achieved under normal incidence excitation, with a hot-spot located near the top surface of the structure. It is shown that the strong field enhancement from this sidewall gap-plasmon mode can be efficiently excited over a broad angular range. The presented plasmonic structure lends itself to implementation in low-cost, chemically stable, easily addressable biochemical sensor arrays providing large optical field enhancement factors. © 2016 Author(s). All article content, except where otherwise noted, is licensed under a Creative Commons Attribution (CC BY) license (<http://creativecommons.org/licenses/by/4.0/>). [<http://dx.doi.org/10.1063/1.4945354>]

Gap-plasmon resonances of metallic nanostructures are rapidly gaining interest due to their extremely high electromagnetic field enhancement which is advantageous in several practical applications including molecular sensing,^{1–5} photovoltaics,^{6,7} photocatalysis,^{8,9} and nanolasers.^{10,11} Metallic nanoparticles on a metallic film (known as the particle-on-mirror geometry) represent an attractive gap plasmon supporting structure because they can be prepared with low-cost methods and exhibit a resonance wavelength that can be controlled reliably by modifying the thickness of a spacer layer.^{12–17} One drawback of the particle-on-mirror structure is the need for high-angle excitation and collection due to the surface-normal polarization of the gap mode. This poses a challenge to the practical implementation of gap plasmons in sensor arrays.

A structure that could overcome this angular restriction is that of a plasmonic nanoparticle (NP) inside a nanohole (NH) in a metallic film. In such systems, hybridized resonances are known to develop.^{18,19} When the NP is close to the sidewall of a NH, the metallic sidewall acts as a mirror enabling the development of a gap plasmon. Early work on a Au NP in an aperture in a gold film demonstrated large field enhancement and enhanced Raman scattering, but did not consider the polarization and excitation angle dependence of the response or its spectral response under normal incidence excitation.²⁰ Moreover, the Au NPs in the study were chemically bound to the bottom of the nanohole, resulting in variable gap sizes and unpredictable resonance frequencies. Jahr *et al.* detected DNA hybridization events using gold nanoparticles in nanoholes in a chromium film but did not utilize gap plasmons.²¹ Cecchini *et al.* investigated surface-enhanced Raman scattering (SERS) from functionalized Au nanoparticles flowing through a nanopore in a gold film,²² but the correlation between particle position and spectral response was not investigated.

^aElectronic mail: kik@creol.ucf.edu



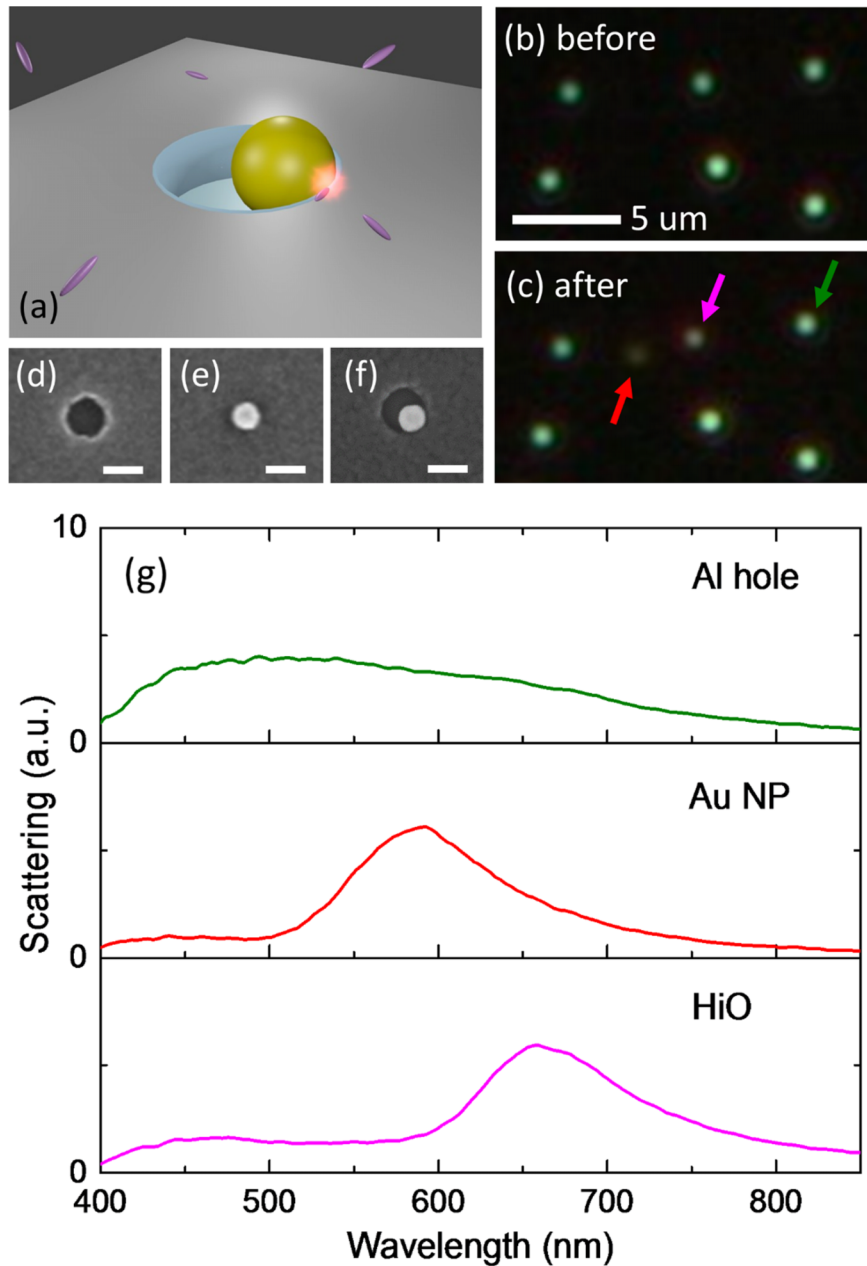


FIG. 1. (a) HiO structure consisting of a Au NP inside a NH in an Al film on a glass substrate, showing the gap-plasmon hot-spot (orange). ((b) and (c)) Darkfield microscopy images before and after Au NP deposition. ((d)–(f)) SEM images of a nanohole, a Au nanoparticle, and a HiO structure. The scale bar in the SEM images represents 100 nm. (g) Scattering spectra of the NH, Au NP on Al, and HiO structure marked by the arrows in (c).

The present work investigates the optical response of a new hybrid Au-Al NP-in-a-hole system. Figure 1(a) shows the proposed structure consisting of a Au nanoparticle located inside a nanohole in an Al film on a glass substrate, covered by a liquid analyte. For brevity, we will refer to this geometry as the *hole-in-one* (HiO) structure. The Au NP touches the oxide-coated Al sidewall enabling the development of a strongly confined gap plasmon mode. A native oxide spacer layer on the Al sidewall leads to a natural minimum gap size, resulting in a predictable resonance wavelength. In addition, the oxide improves thermal and mechanical stability and removes the need for organic spacer molecules that could introduce a background signal in biochemical sensing with the structure.²³ This new Au-Al hybrid geometry provides a reliable plasmonic hot-spot and enables

facile normal-incidence excitation and detection. This configuration could be used to detect optical signatures from molecules adsorbed on the structure or diffusing into the hot-spot.

A combination of nanosphere lithography and NP deposition was used to fabricate HiO structures. First, 110 nm diameter polystyrene (PS) beads were drop coated onto a glass coverslip, followed by thermal evaporation of a 37 nm Al film (deposition rate $\sim 5 \text{ \AA/s}$). Exposure to air leads to the formation of a few-nm thick native oxide on all exposed Al surfaces. Removal of the PS beads leaves behind ~ 110 nm diameter holes in the Al film. Subsequently, 60 nm diameter Au particles were drop coated onto the sample from colloidal solution, placing a NP in a small fraction of the holes. Nanoholes containing a NP were located using darkfield microscopy before and after drop coating of the colloidal Au NP solution.

Figure 1(b) shows a darkfield microscopy image of a typical sample region after hole formation but before Au NP deposition. The green scattering spots originate from the nanoholes in the Al film. A typical Scanning Electron Microscopy (SEM) image of a NH is shown in Fig. 1(d). Figure 1(c) presents a darkfield microscopy image of the same area taken after Au NP deposition. Note that an additional pale-yellow scattering spot appears (red arrow). This feature corresponds to an isolated Au NP on the Al surface, as seen in the SEM image in Fig. 1(e). The hole indicated by the magenta arrow shows a reduced brightness and a more pale yellow or orange color. Similar changes in optical signature were observed at different locations on the sample. Figure 1(f) shows an SEM image of one of these structures, revealing a HiO structure containing a gold nanoparticle in close contact with the sidewall of a circular hole in the Al film. This off-center particle configuration seems to be favorable, which we attribute to capillary forces acting on the particle during the drying process after drop-coating. Note that while the presented fabrication steps produce relatively few HiO structures, the yield may be improved using capillary force mediated techniques similar to the templated self-assembly method.^{24,25}

Figure 1(g) presents darkfield scattering spectra obtained from the structures indicated by the arrows in Fig. 1(c). The spectral response under off-normal excitation was collected at N.A. = 0.75 and was analyzed using selective area darkfield spectroscopy. Spectra were calculated using the formula $I = (I_{NS} - I_{ref})/I_{ref}$, where I_{NS} and I_{ref} are the dark-current corrected signals from the structure and a nearby Al area, respectively. The nanohole shows a broad featureless scattering spectrum, with a maximum in the blue-green spectral region. In contrast, the scattering spectrum of the isolated Au NP shows a prominent resonance peak ~ 585 nm with a full width at half maximum (FWHM) of ~ 105 nm, corresponding to a gap plasmon resonance between the Au NP and the oxidized Al film.¹⁶ The HiO spectrum from the structure shown in Fig. 1(f) shows a scattering peak at ~ 660 nm with a similar scattering intensity and linewidth as the isolated Au NP. This suggests that the HiO structure supports a gap-plasmon mode, with a modified spectral response due to the curvature and finite height of the Al sidewall.

Figure 2(a) shows a darkfield microscopy image of the HiO, Au NP, and nanohole labelled by the arrows in Fig. 1(c). The image was rotated clockwise by 90° for presentation purposes. The isolated Au NP shows the characteristic red ring-shaped scattering pattern associated with surface-normal gap plasmon resonances of single Au NPs on metallic substrates.^{1,15,16} Figure 2(b) shows the same structures with a linear analyzer inserted in the collection path of the microscope at six different analyzer angles. This transforms the ring-shaped scattering pattern of the isolated Au NP into a dumbbell-shaped image, due to the radial polarization of the scattered light from the gap plasmon resonance. The NH and HiO structures remain circularly symmetric upon rotation of the analyzer, demonstrating that these scattering features are not dominated by a surface-normal polarization, a first indication that the HiO structure is better suited for normal incidence excitation and collection than the isolated Au NP. As the analyzer is rotated, the scattering color of the nanohole remains unchanged while the HiO structure exhibits a clear color shift varying between red and green. Figure 2(c) presents an SEM image of the sample area shown in Figs. 2(a) and 2(b). A corresponding zoom-in image of the HiO structure is shown in the left inset in Fig. 2(d).

The polar plot in Fig. 2(d) shows the recorded peak scattering intensity as a function of analyzer angle, revealing maximum scattering at an angle of $\sim 60^\circ$. The SEM image of this HiO structure in Fig. 2(d) shows that the Au NP touches the oxidized Al sidewall of the nanohole at this same angle, corresponding to the symmetry axis of the structure (dashed white line). The two spectra

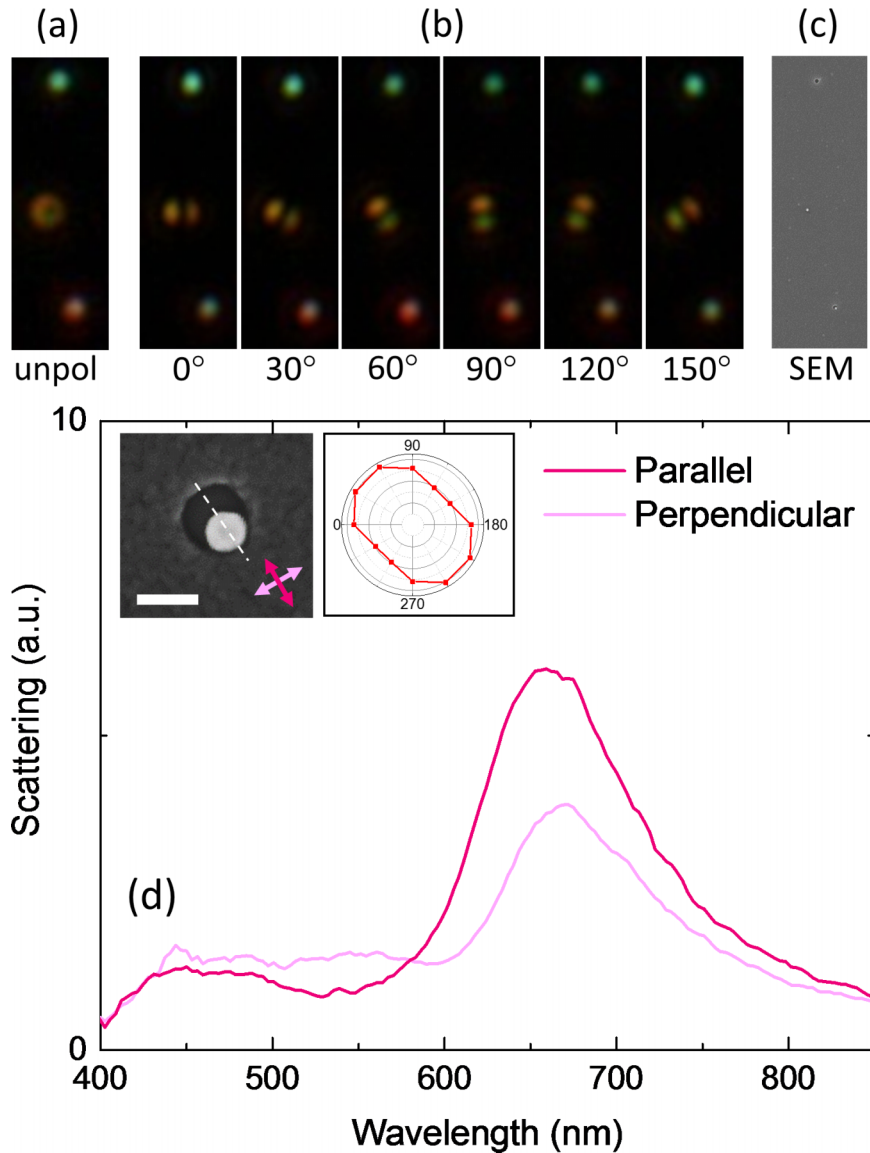


FIG. 2. (a) Darkfield microscopy image of the NH (top), Au NP (middle), and HiO structure (bottom) from Fig. 1(b) and (b) of the same structures but with a linear analyzer inserted in the collection path. (c) Corresponding SEM image. Images ((a)–(c)) are $\sim 2.5 \mu\text{m}$ wide. (d) Scattering spectra of the HiO structure collected with the analyzer parallel and perpendicular to the symmetry axis (dashed white line) indicated, respectively, by the magenta arrows. The scale bar is 100 nm. The polar plot shows the peak scattering intensity as a function of analyzer angle.

shown in Fig. 2(d) were recorded with the analyzer oriented along the light and dark magenta arrows in the SEM image. Note that the HiO structure indeed appears red in Fig. 2(b) when the analyzer is aligned with the symmetry axis. The observed variation in color and scattering intensity upon rotation of the analyzer is attributed to the polarization direction of the gap plasmon which is predominantly along the symmetry axis of the structure. Consequently, the scattered light is predominantly polarized along this axis, and rotating the analyzer angle away from this axis will reduce the gap-plasmon related contribution to the scattering spectrum and reduce the red gap-plasmon related contribution in the collected image.

To investigate the optical response of the HiO structures under normal incidence excitation, transmission measurements were carried out. Figure 3(a) presents the normal-incidence transmission spectra of the HiO structure and the nanohole marked by the magenta and green arrows in

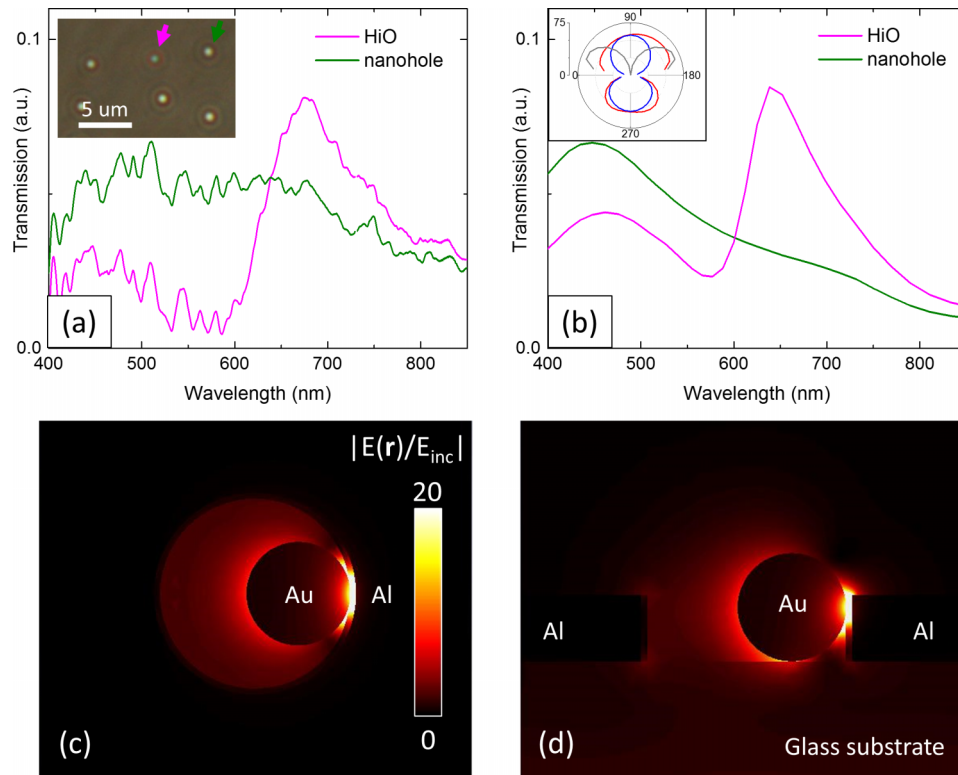


FIG. 3. ((a) and (b)) Measured and simulated transmission spectra of a HiO structure and an isolated NH. The measured spectra were obtained from the HiO structure and NH in Al marked by the magenta and green arrows in the transmission microscopy image inset. ((c) and (d)) Electric field distribution of a HiO structure under normal incidence excitation at the main resonance frequency. The field cuts correspond to (c) a plane along the surface at the height where the Au NP touches the oxidized Al sidewall and (d) a surface-normal plane along the HiO symmetry axis. The polar plot in (b) shows the field enhancement factor in the NP-oxide junction region of the HiO structure as a function of excitation angle along (red curve) and normal to (blue curve) the HiO symmetry axis, and of a Au NP on an Al film (gray curve).

Fig. 1(c). The same background subtraction procedure used to calculate scattering spectra was applied. The inset shows the corresponding transmission microscopy image. The transmission spectrum of the nanohole is broad and virtually featureless, similar to the NH scattering spectrum in Fig. 1(g). The transmission spectrum of the HiO, on the other hand, shows a region of enhanced transmission at ~ 670 nm with a FWHM linewidth of ~ 140 nm. This matches the scattering peak of the HiO structure in Fig. 1(g) suggesting that the sidewall gap plasmon mode is successfully excited under normal incidence illumination.

To clarify the nature of the transmission peak in Fig. 3(a), numerical simulations were carried out.²⁶ The simulations consider a 60 nm diameter Au NP in a 110 nm diameter nanohole in a 37 nm thick Al film on a glass substrate with the Au NP touching the sidewall. A 3.4 nm thick native Al_2O_3 layer is assumed to be present on the sidewalls of the NH.¹⁶ Literature data were used for the dielectric functions.^{27–29} Figure 3(b) shows the simulated transmission spectra of a HiO structure and of an isolated nanohole in an Al film. The transmission spectrum of the HiO structure exhibits a peak resonance wavelength of ~ 645 nm and a FWHM linewidth of ~ 120 nm while the simulated nanohole transmission spectrum is broad and featureless, both in good agreement with the measured results. The good correspondence between experiment and simulation in Figs. 3(a) and 3(b) allows us to estimate the experimentally achieved field enhancement.

Figures 3(c) and 3(d) show the simulated electric field enhancement factor $|E(\mathbf{r})/E_{\text{inc}}|$ of the HiO structure at 625 nm, corresponding to the main resonance frequency, where $E(\mathbf{r})$ is the simulated electric field distribution and E_{inc} the amplitude of the incident wave. The top view in Fig. 3(c) represents a field cut at the height where the NP touches the sidewall, and the side view in Fig. 3(d)

shows a field cut normal to the sample surface along the HiO symmetry axis. The hot-spot occurs near the sample surface and is extremely confined near the junction between the Au NP and the oxidized sidewall of Al film, with a peak field enhancement factor as high as 52. The field distribution closely resembles the gap-plasmon of a NP-on-a-mirror structure, but with a predominant field polarization parallel to the sample surface. The polar plot in Fig. 3(b) shows the electric field enhancement factor at the junction of the HiO structure under excitation at 625 nm with the incident electric field polarized along the HiO symmetry axis, as a function of the angle of incidence, with 90° corresponding to normal incidence top illumination. The HiO structure produces a large field enhancement factor over a wide range of angles in the surface-normal planes oriented along (red curve) and normal to (blue curve) the HiO symmetry axis, under both top and bottom illuminations. The gray curve shows the corresponding data for a Au NP on a flat Al film under TM excitation. The HiO structure produces significantly larger field enhancement factors for near-normal excitation angles and offers a more angle-invariant response compared to that of the NP-on-mirror geometry. Note that the gap-plasmon mode of the HiO structure can be excited through the glass substrate, enabling optical interrogation even in the presence of a strongly absorbing analyte solution. The omnidirectional excitation of strong gap-plasmon enhanced local electric fields makes the presented HiO geometry ideal for applications that rely on normal incidence optical inspection of large area arrayed sensor elements.

In conclusion, we have investigated hybrid hole-in-one nanostructures consisting of a gold nanoparticle in a nanopore in an aluminum film. The structure supports a strong gap-plasmon resonance with convenient optical access to the hot-spot and it can be fabricated using simple and low-cost methods. The self-limiting growth of a 3-4 nm thick native Al_2O_3 layer introduces a natural minimum spacing between the Au and Al surfaces, reducing variability in gap size and enabling a reproducible resonance wavelength. The oxide layer thickness can be increased uniformly to further control the resonance frequency of the structure through anodization.¹⁶ A prominent plasmon resonance peak in both scattering and normal incidence transmission spectra indicates that gap-plasmons supported by the HiO structures can be excited and detected at high and near-normal angles of incidence. Simulations of the structure match the experimental results and suggest a maximum field enhancement factor of ~ 52 under normal incidence illumination. The structure generates strong field enhancement over a wide range of excitation angles with a hot-spot near the film surface. This is attractive for optical sensing applications such as SERS and fluorescence sensing^{30,31} that leverage the enhanced electric field and the small optical mode volume. The nanohole also acts as a zero-mode-waveguide ensuring reduced excitation of fluorescence in the analyte, reduced transmission of any excited fluorescence back to the illumination side, and providing a small sampling volume which could allow the use of undiluted analyte solutions.³¹⁻³⁶ These traits make the HiO structure ideal for implementation as a sensing element in large-area ultrasensitive biochemical sensor arrays.

This work has been made possible thanks to the financial support from the National Science Foundation (No. NSF CHE-1213182).

- ¹ S. Y. Chen, J. J. Mock, R. T. Hill, A. Chilkoti, D. R. Smith, and A. A. Lazarides, *ACS Nano* **4**, 6535 (2010).
- ² W. Kubo and S. Fujikawa, *Nano Lett.* **11**, 8 (2011).
- ³ S. Mubeen, S. P. Zhang, N. Kim, S. Lee, S. Kramer, H. X. Xu, and M. Moskovits, *Nano Lett.* **12**, 2088 (2012).
- ⁴ L. Li, T. Hutter, U. Steiner, and S. Mahajan, *Analyst* **138**, 4574 (2013).
- ⁵ J. M. Hoffmann, H. Janssen, D. N. Chigrin, and T. Taubner, *Opt. Express* **22**, 14425 (2014).
- ⁶ S. A. Mann and E. C. Garnett, *ACS Photonics* **2**, 816 (2015).
- ⁷ H. I. Park, S. Lee, J. M. Lee, S. A. Nam, T. Jeon, S. W. Han, and S. O. Kim, *ACS Nano* **8**, 10305 (2014).
- ⁸ Z. W. Liu, W. B. Hou, P. Pavaskar, M. Aykol, and S. B. Cronin, *Nano Lett.* **11**, 1111 (2011).
- ⁹ M. A. Mahmoud and M. A. El-Sayed, *ChemCatChem* **6**, 3540 (2014).
- ¹⁰ R. F. Oulton, V. J. Sorger, T. Zentgraf, R. M. Ma, C. Gladden, L. Dai, G. Bartal, and X. Zhang, *Nature* **461**, 629 (2009).
- ¹¹ Y. J. Lu, C. Y. Wang, J. Kim, H. Y. Chen, M. Y. Lu, Y. C. Chen, W. H. Chang, L. J. Chen, M. I. Stockman, C. K. Shih, and S. Gwo, *Nano Lett.* **14**, 4381 (2014).
- ¹² J. J. Mock, R. T. Hill, A. Degiron, S. Zauscher, A. Chilkoti, and D. R. Smith, *Nano Lett.* **8**, 2245 (2008).
- ¹³ M. W. Knight, Y. P. Wu, J. B. Lassiter, P. Nordlander, and N. J. Halas, *Nano Lett.* **9**, 2188 (2009).
- ¹⁴ C. Ciraci, R. T. Hill, J. J. Mock, Y. Urzhumov, A. I. Fernandez-Dominguez, S. A. Maier, J. B. Pendry, A. Chilkoti, and D. R. Smith, *Science* **337**, 1072 (2012).
- ¹⁵ M. Hu, A. Ghoshal, M. Marquez, and P. G. Kik, *J. Phys. Chem. C* **114**, 7509 (2010).

- ¹⁶ C. Lumdee, S. Toroghi, and P. G. Kik, *ACS Nano* **6**, 6301 (2012).
- ¹⁷ T. Ding, D. Sigle, L. W. Zhang, J. Mertens, B. de Nijs, and J. Baumberg, *ACS Nano* **9**, 6110 (2015).
- ¹⁸ E. Prodan and P. Nordlander, *J. Chem. Phys.* **120**, 5444 (2004).
- ¹⁹ F. I. Baida, A. Belkhir, D. Van Labeke, and O. Lamrous, *Phys. Rev. B* **74**, 205419 (2006).
- ²⁰ H. Wei, U. Hakanson, Z. L. Yang, F. Hook, and H. X. Xu, *Small* **4**, 1296 (2008).
- ²¹ N. Jahr, M. Anwar, O. Stranik, N. Hadrich, N. Vogler, A. Csaki, J. Popp, and W. Fritzsche, *J. Phys. Chem. C* **117**, 7751 (2013).
- ²² M. P. Cecchini, A. Wiener, V. A. Turek, H. Chon, S. Lee, A. P. Ivanov, D. W. McComb, J. Choo, T. Albrecht, S. A. Maier, and J. B. Edel, *Nano Lett.* **13**, 4602 (2013).
- ²³ C. Lumdee, B. Yun, and P. G. Kik, *J. Phys. Chem. C* **117**, 19127 (2013).
- ²⁴ Y. Cui, M. T. Bjork, J. A. Liddle, C. Sonnichsen, B. Boussert, and A. P. Alivisatos, *Nano Lett.* **4**, 1093 (2004).
- ²⁵ J. A. Fan, K. Bao, L. Sun, J. M. Bao, V. N. Manoharan, P. Nordlander, and F. Capasso, *Nano Lett.* **12**, 5318 (2012).
- ²⁶ CST Microwave Studio®, Computer Simulation Technology, Darmstadt, Germany.
- ²⁷ E. D. Palik and G. Ghosh, *Handbook of Optical Constants of Solids* (Academic Press, Orlando, London, 1985).
- ²⁸ P. B. Johnson and R. W. Christy, *Phys. Rev. B* **6**, 4370 (1972).
- ²⁹ T. Lichtenstein, *Handbook of Thin Film Materials* (University of Rochester, Rochester, NY, 1979).
- ³⁰ J. D. Jackson, *Classical Electrodynamics*, 3rd ed. (Wiley, New York, 1999).
- ³¹ M. J. Levene, J. Korlach, S. W. Turner, M. Foquet, H. G. Craighead, and W. W. Webb, *Science* **299**, 682 (2003).
- ³² K. T. Samiee, J. M. Moran-Mirabal, Y. K. Cheung, and H. G. Craighead, *Biophys. J.* **90**, 3288 (2006).
- ³³ J. M. Moran-Mirabal and H. G. Craighead, *Methods* **46**, 11 (2008).
- ³⁴ J. Larkin, M. Foquet, S. W. Turner, J. Korlach, and M. Wanunu, *Nano Lett.* **14**, 6023 (2014).
- ³⁵ A. G. Brolo, E. Arctander, R. Gordon, B. Leathem, and K. L. Kavanagh, *Nano Lett.* **4**, 2015 (2004).
- ³⁶ B. Nie, C. L. He, and L. J. Liu, *J. Raman Spectrosc.* **44**, 1512 (2013).